



Research Report  
**BrainWorks 1991-01**  
ISSN 1615-2042

## **Binaural Interaction in the Nucleus Laminaris of the Barn Owl: A Quantitative Model**

**Sonja Grün, Hermann Wagner,  
Catherine Carr, Ad Aertsen**

Neurobiology & Biophysics  
Institute for Biology 3  
Albert-Ludwigs-University  
Freiburg, Germany  
<http://www.brainworks.uni-freiburg.de>



*Impressum*

**BrainWorks**

ISSN 1615-2042

*Herausgeber/Publisher:*

Neurobiologie & Biophysik  
Institut für Biologie III  
Albert-Ludwigs-Universität Freiburg  
Deutschland

Neurobiology & Biophysics  
Institute of Biology III  
Albert-Ludwigs-University Freiburg  
Germany

*Verlagsort/City:* Freiburg im Breisgau

*Postadresse/postal adress:*

Schänzlestr. 1  
79104 Freiburg  
Germany

*Tel:* +49 761 203-2786

*FAX:* +49 761 203-2860

*Email:* [brainworks@biologie.uni-freiburg.de](mailto:brainworks@biologie.uni-freiburg.de)

*Website:* <http://www.brainworks.uni-freiburg.de>

## **Binaural Interaction in the Nucleus Laminaris of the Barn Owl: a Quantitative Model**

Sonja Grün<sup>1,3</sup>, Hermann Wagner<sup>1,4</sup>, Catherine Carr<sup>2</sup> and Ad Aertsen<sup>1,5</sup>

<sup>1</sup>Max-Planck Inst. for Biological Cybernetics,  
Spemannstrasse 38, D-7400 Tübingen, Germany

<sup>2</sup>Dept. of Zoology, University of Maryland,  
College Park, MD 20742-4415, USA

July 5th, 1991

Correspondence to: Dr. Sonja Grün  
Max-Planck Institute for Brain Research  
Dept. of Neurophysiology  
60528 Frankfurt/Main  
Germany  
tel: +49-69-96769-336  
fax: +49-69-96769-327  
gruen@mpih-frankfurt.mpg.de

---

present addresses:

<sup>3</sup>Max-Planck Inst. for Brain Research, Dept. of Neurophysiology, Deutschordenstr. 46, D-60528 Frankfurt/Main, Germany; <sup>4</sup>Dept. of Zoology and Animal Physiology, Inst. of Biology II, RWTH, Kopernikusstr. 16, D-52074 Aachen, Germany; <sup>5</sup>Dept. of Neurobiology and Biophysics, Inst. of Biology III, Albert-Ludwigs-University, Schänzlestr. 1, D-79104 Freiburg, Germany

## Abstract

A quantitative, neuronal model is proposed for the computation of interaural time difference (ITD) in the auditory system of the barn owl. The model uses a general, probabilistic approach, and is composed of two stages, the characteristics of which are based on anatomical and physiological evidence. Excitatory inputs from both ears, phase-locked to the waveform of tonal stimuli, together with phase-independent inhibitory inputs are summated linearly. The result is transformed into a probability of spike generation by a sigmoid nonlinearity, constituting a stochastic, 'soft' threshold with saturation. The model incorporates inhibition as a control parameter on the non-linearity, and includes the usual crosscorrelation-type models as a special case. It has a minimum number of parameters, the values of which can be estimated from physiological data in a straightforward manner. This simple, general model accounts for the binaural response properties of physiologically recorded neurons. In particular, it explains the experimentally observed ITD-tuning and the increase of phase-locking from input to output neurons. The model predicts that a decrease in inhibition causes a non-monotonic change in sensitivity to ITD.

**Keywords:** sound localization/neuronal model/coincidence detection/synchrony of firing/role of inhibition

**Abbreviations:** ITD, interaural time difference; IPD, interaural phase difference; NM, nucleus magnocellularis; NL, nucleus laminaris; PH, period histogram.

## 1 Introduction

Unlike the visual system, the auditory system does not comprise a map of external space on its sensory epithelium. Instead, the location of a sound source is computed in the central nervous system. One of the primary cues for determining the azimuth of a sound source is the interaural time difference (ITD). As early as 1948, Jeffress (1) proposed an influential model of ITD-detection, composed of two main elements: delay lines followed by coincidence detection. Evidence - partly anatomical, partly physiological - for these elements was obtained in a third-order nucleus, the medial superior olive in mammals (2-4), and the nucleus laminaris in birds (5-8).

Most attempts to model coincidence detection took the form of a crosscorrelation: some kind of multiplication, followed by temporal integration (3, 9, 10; for a review see 11). In contrast to this, we adopted a more general, probabilistic approach. A regular neuron model (e.g. 12, 13) formed the basis of a quantitative model of binaural interaction that incorporates anatomical and physiological data from the barn owl's auditory brainstem nuclei (7, 8).

## 2 Physiology and Anatomy of the Owl's Auditory Brainstem

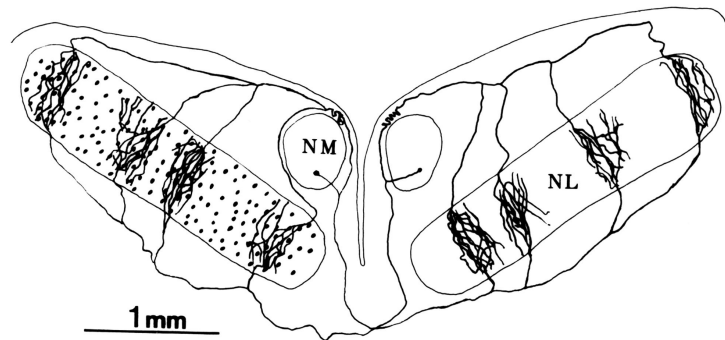


**Figure 1:** Connections from nucleus magnocellularis (NM) to nucleus laminaris (NL). The drawing shows a frontal view with two NM somata and axons stained intracellularly with HRP. The NL is very large and contains regularly distributed neurons with short, stubby dendrites (14). Somata of NL neurons, stained with an antibody against calretinin, are indicated by dots. Each NM neuron projects bilaterally to the NL. After leaving NM, each axon divides into two primary branches. The ipsilateral branch travels along the dorsal edge of the ipsilateral NL until it reaches its isofrequency lamina, and fans out into several secondary collaterals, each of them dividing further and running from dorsal to ventral through the nucleus. The contralateral primary branch crosses the midline to reach the ventral border of the contralateral NL, where it also divides into secondary collaterals that enter the NL and run from ventral to dorsal through the nucleus. Thus, ipsilateral and contralateral axon arbors interdigitate within NL.

In the auditory system of the barn owl, ITD is analyzed in a separate, hierarchically organized network, the 'time pathway'. The anatomical and physiological features of the first two stations of this pathway, the cochlear nucleus magnocellularis (NM) and the nucleus laminaris (NL), the first locus of binaural interaction, make them particularly suited for the computation of ITD (Fig. 1).

Neurons show a high spontaneous activity (100 spikes/s), and a purely monaural and largely level-independent response to acoustic stimuli. For frequencies up to 9 kHz, the response to tones depends on the stimulus phase ('phase-locking'), as can be demonstrated by presenting the spike counts as a function of time, with the time base equal to the period of the stimulus tone: the 'period histogram' (PH, Fig. 2). A quantitative measure for the degree of phase-locking is the 'vector strength' (2). NM neurons project bilaterally to the NL, with axon collaterals of many NM neurons running in parallel through an isofrequency lamina, and ipsilateral and contralateral axon arbors interdigitating (Fig. 1). Thus, when a micro-electrode is advanced along the axon collaterals, the preferred phase of the PHs increases in the ipsilateral axons and decreases in the contralateral axons. Hence, NM axons in the NL can be thought of as delay lines (7, 8), constituting the first element in the Jeffress model. Finally, recordings of a local field potential, the 'neurophonics', exhibit phase-locking properties and a change of preferred phase with electrode depth that are comparable to the equivalent responses of single axons (6,7), indicating that NM afferents respond in strong synchrony. NL neurons are contacted on their short, stubby dendrites by about 100 terminals from each NM (8). In addition, each NL neuron receives about 50 GABA-ergic terminals of unknown origin (14). NL neurons respond to monaural and binaural stimuli; the monaural response is about half the binaural response at the preferred ITD, and generally larger than the response to an

unfavorable ITD. NL neurons phase-lock better to monaural stimuli than their NM inputs do (8). The binaural response varies with ITD in a cyclic fashion, described by the 'ITD-curve' (Fig. 4a). Its period equals the period of the stimulating tone. The peaks of the ITD-curve occur at the neuron's preferred interaural phase difference (IPD; 15). These characteristics suggest, that the neurons compute ITD from IPD. The peaks of the left and right monaural PHs occur at different times within the stimulus cycle, the time difference being equal to the neuron's preferred ITD. Hence, it was proposed that NL neurons act as coincidence detectors, the second element in the Jeffress model (6-8).

### 3 A Quantitative Model of Binaural Interaction

The aim of our model is to describe the stochastic transformation taking place between the phase-dependent probabilities of firing of the NM and the NL neurons, as statistically expressed in their PHs. The anatomical and physiological findings described above constitute the biological basis of this model; their quantitative characteristics are incorporated in the numerical calculations. Both in view of the nature of the underlying mechanism, and for reasons of mathematical convenience, our model is formulated in terms of phase, rather than time. Hence, our model calculations will refer to IPD, instead of ITD; for any particular frequency, however, the transformation of one to the other is trivial (Fig. 4a).

Following the literature on neural modelling (e.g. 12, 13), we assume that computations in NL neurons take place in two stages: (1) linear integration in the somato-dendritic compartment, taking the form of a simple summation of excitatory NM inputs from both sides and inhibitory inputs of unknown origin, and (2) subsequent nonlinear transformation of the resulting 'generator potential' into the probability of spike generation at the output.

Consider first the various contributions to the input of the NL neuron. The strong synchrony of firing among NM axons from each side, together with the very short dendrites of NL cells, argue for the assumption that the contribution to a particular NL neuron of the many excitatory NM inputs from each side can be represented by the PH of a single representative NM neuron. This assumption, which equates the average over a homogeneous ensemble of neurons with the average over a homogeneous ensemble of trials involving any one of these neurons, is usually referred to as 'quasi-ergodic', following the physical literature. Thus, at the first stage of the model, summation of both NM PHs  $X_i(\phi)$  ( $i = 1, 2$ : left and right), and the inhibition  $X_3(\phi)$  results in the 'generator potential':

$$Y(\phi) = X_1(\phi) + X_2(\phi) - X_3(\phi) \quad (1)$$

In our numerical calculations, we approximated each of the two NM PHs ( $i = 1, 2$ ) by a sinusoidal modulation around a baseline (Fig. 2, left):

$$X_i(\phi) = a_i + b_i \cdot \cos(\phi + \psi_i) \quad (2)$$

Thus, the firing probability of each NM neuron is characterized by three parameters: 1)  $a$ , the mean firing rate or 'base rate', 2)  $b$ , the stimulus-induced modulation amplitude, and 3)  $\psi_i$ , the preferred phase.

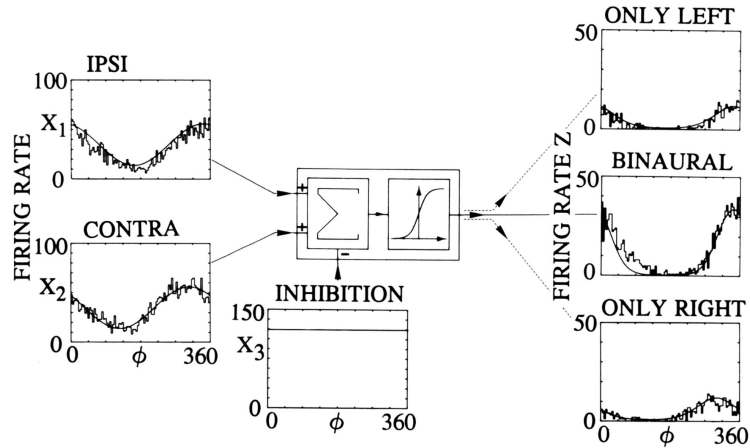


**Figure 2:** Schematic diagram of the model NL neuron, with input and output period histograms. The model neuron is composed of two stages: linear summation of the inputs  $X_i$ , followed by a nonlinear transformation of the 'generator potential'  $Y$  into the probability of firing  $Z$  at the output. The excitatory inputs ( $X_1 = \text{ipsi}$ ,  $X_2 = \text{contra}$ ) are shown on the left. Bar graphs represent experimental period histograms from NM neurons with best frequency of about 4400 Hz. On the x-axis is plotted the stimulus phase  $\psi$ . The histograms are divided into 90 phase-bins, corresponding to a binwidth of some 2.5  $\mu\text{sec}$ . The vector strengths of the ipsi and contra input PHs are  $v = 0.34$  and  $v = 0.294$ , respectively. Continuous curves represent the sinusoidal approximations (Equ. 1;  $a = 34.8$  spikes/phase-bin,  $b = 21.0$  spikes/phase-bin;  $v = 0.302$ ). The uniform period histogram (bottom center) depicts the phase-independent inhibitory input  $X_3$ . On the right are the monaural (top ( $\psi = 342.7^\circ$ ,  $v = 0.623$ ) and bottom ( $\psi = 299.2^\circ$ ,  $v = 0.589$ )) and binaural period histogram ( $\psi = 353.2^\circ$ ,  $v = 0.624$ ) at preferred ITD ( $= -30\mu\text{sec}$ ) (center) of an NL neuron with best frequency of also about 4400 Hz. Using the above values for the input parameters, the inhibition  $\theta$  and the model parameters  $\alpha$  and  $d$  were estimated from the experimental monaural NL period histograms. The resulting values ( $\theta = 119$  spikes/phase-bin,  $\alpha = 0.066$  phase-bins/spike,  $d = 88.5$  spikes/phase-bin) were used to calculate the model NL responses (continuous curves). The simulated binaural PH at best IPD ( $= -43.5^\circ$ ; mean phase  $\psi = 342.7^\circ$ ) has a vector strength of  $v = 0.752$ . In the simulated monaural PHs  $v$  was 0.545. Observe the good agreement between physiological data and model predictions.

These three parameters can be estimated from the physiological data in a straightforward manner. The base rate  $a$  is simply the mean value of the NM period histogram. For a truly sinusoidal PH ( $a > b$ ), the vector strength  $v$  can be expressed in  $a$  and  $b$  as  $v = b/2a$ . Hence,  $b$  can be estimated from the mean rate and the vector strength by  $b = 2a \cdot v$ . Finally, the preferred phase of the NM neuron is composed of two contributions, one external and the other internal:  $\psi_i = \varphi_{0i} + \varphi_i$ . The external phase shift  $\varphi_{0i}$  corresponds to the delay from the sound source to the ear, and is set by the experimenter. The internal phase shift  $\varphi_i$  reflects neural delays. Since we assume that the computations of NL neurons are instantaneous, i.e. not introducing an additional phase-shift, the internal phase shift  $\varphi_i$  of the NM neuron can be taken identical to the phase of the peak response in the corresponding monaural PH of the NL neuron.

We stress that the sinusoidal approximation of the firing probability of NM neurons primarily serves reasons of economy and mathematical convenience. It is in no way essential for the proposed model of binaural interaction in NL neurons. In fact, our model performs equally well when operating upon the 'raw' experimental input PHs in the form of arrays of actual bin counts.

Nothing being known about the physiological characteristics of the inhibitory inputs nor

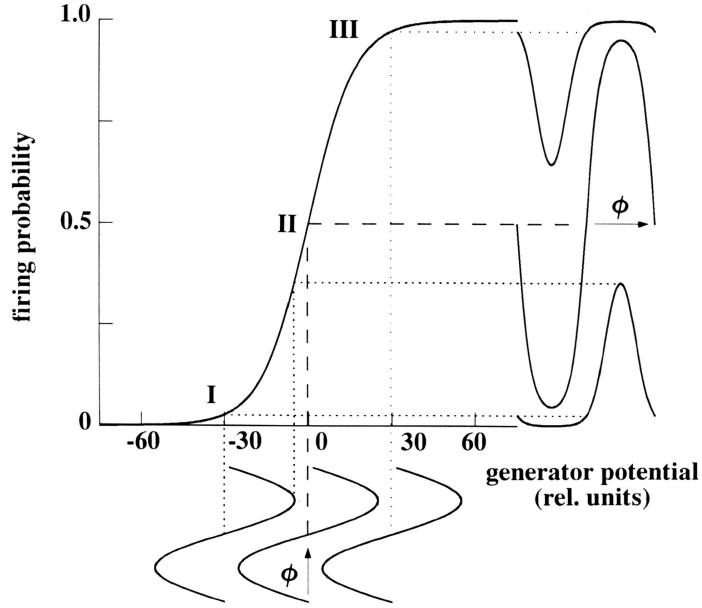


**Figure 3:** Sigmoid nonlinearity, transforming 'generator potential' into firing probability. The dotted and dashed lines indicate how single input values are transformed. The influence of the operating point is illustrated for three sinusoidal inputs at different mean levels, shown below the x-axis; the resulting outputs are displayed on the right. Observe how the operating point, set by the inhibition and the mean input rate, determines the type and amount of distortion, depending on whether it is located in the expansive region (I), in the quasi-linear region (II) or in the compressive region (III).

of their site of origin, we make the weakest possible assumption: the inhibition is taken to be phase-independent (i.e. no phase-locking):  $X_3(\phi) = \theta$ . By inserting this variable and Equ. 2, and assuming symmetry of the inputs from both sides ( $a_1 = a_2$  and  $b_1 = b_2$ ), Equ. 1 can be rearranged to yield the 'generator potential':

$$Y(\phi) = 2a - \theta + 2b \cdot \cos(\psi_{\text{diff}}) \cdot \cos(\psi_{\text{sum}}) \quad (3)$$

$$\text{with } \psi_{\text{diff}} = (\psi_1 - \psi_2)/2 = (\varphi_{01} + \varphi_1 - \varphi_{02} - \varphi_2)/2 = \text{IPD}/2 + (\varphi_1 - \varphi_2)/2$$

$$\text{and } \psi_{\text{sum}} = \phi + (\psi_1 + \psi_2)/2 = \phi + (\varphi_{01} + \varphi_1 + \varphi_{02} + \varphi_2)/2$$

Thus,  $Y(\phi)$  is again a sinusoidal function of stimulus phase, with the stimulus-independent mean value  $2a - \theta$ . The stimulus-dependent contribution is the product of two terms: one depends on the stimulus phase ( $\cos(\phi_{\text{sum}})$ ), the other is a modulating term ( $2b \cdot \cos(\psi_{\text{diff}})$ ), which only depends on IPD. If the preferred phases from both sides are equal,  $\cos(\psi_{\text{diff}})$  is 1 and the modulation amplitude reaches a maximum of  $2b$ . If, on the other hand, both inputs are  $180^\circ$  out of phase, the modulation amplitude equals zero and, hence, only the constant term remains.

In the second stage of the model,  $Y(\phi)$  is transformed by an algebraic, sigmoid nonlinearity to yield the period histogram of the NL neuron:

$$Z(\phi) = \frac{d}{1 + \exp(-\alpha \cdot Y(\phi))} \quad (4)$$

The sigmoid function is composed of a form factor, characterized by the slope  $\alpha$ , that describes the probability of spike generation, and a scaling factor  $d$ , which transforms firing probability into spike rate (Fig. 3). Three different operating regimes can be distinguished: an expansive region (I), a quasi-linear region around the point of inflexion (II), and a compressive region (III). Thus, the distortion of the period histogram of the NL neuron depends on the operating point on the nonlinearity, set by the mean value of the 'generator potential'.

## 4 Parameter Estimation, Test of the Model, and Predictions

In order to evaluate the performance of the model quantitatively, we first had to determine the input parameters ( $a, b, \psi_i, \theta$ ) and the model parameters ( $\alpha, d$ ). Lacking simultaneous recordings from an NL neuron and its NM input neurons, we selected typical NM period histograms as input, and calculated the parameters  $a, b$  and  $\psi$  as described before. Using these estimates, we calculated the inhibition and the model parameters ( $\alpha, d$ ) of an NL neuron with similar best frequency from its monaural period histograms by solving the monaural version of Equ. 4 at three appropriately chosen phase angles (16, 17). After all parameters were specified, the binaural response of the NL neuron at the preferred IPD was calculated from Equ. 4. Thus, the predicted binaural NL response is not obtained from some fitting procedure to the binaural histogram, but is the result of an analytical expression. Observe that the histogram waveform, the maximal spike rate, the mean phase and the vector strength of the model responses are almost identical to their experimental counterparts (Fig. 2). Also in accordance with the experimental results, the model NL neuron exhibits a reduced firing rate, an asymmetric distortion of the PH and, hence, a considerably stronger phase-locking than the NM neuron. The latter phenomenon is a direct result of the shape of the nonlinearity. Inspection of PHs of NL neurons strongly suggests that the expansive region of the sigmoid curve (Fig. 3, I) is the normal physiological operating regime (2, 8), weighting responses at preferred phases more strongly than responses at non-preferred phases.

As shown in Equ. 3, the response of the model NL neuron depends on IPD. This dependence is quantified by integrating the spike activity in the binaural period histogram for different IPDs:

$$\bar{Z}(\text{IPD}) = \int_{0^\circ}^{360^\circ} Z(\phi, \text{IPD}) d\phi \quad (5)$$

A plot of the resulting values as a function of IPD (the 'IPD-curve') is shown in Fig. 4a (lower curve); its experimental counterpart, the ITD-curve, is also given in Fig. 4a (upper curve). Clearly the two curves agree very well. Both show definite tuning, with identical preferred IPD. In each case, the locations of maximal and minimal responses are separated by  $180^\circ$ , and the monaural responses are about half of the maximum. Finally, the minimum of each curve coincides with the level of spontaneous activity, with the only difference that the predicted spontaneous activity is higher than the experimental value.

In addition to explaining established experimental facts, we can also use the model to suggest new experiments, and to predict hitherto unknown properties of the system. Thus, by varying different parameters, we arrived at a number of quantitative predictions regarding the behavior of NL neurons under various physiological manipulations (16, 17). An interesting example is provided by varying the level of inhibition. The result is a shift of the operating

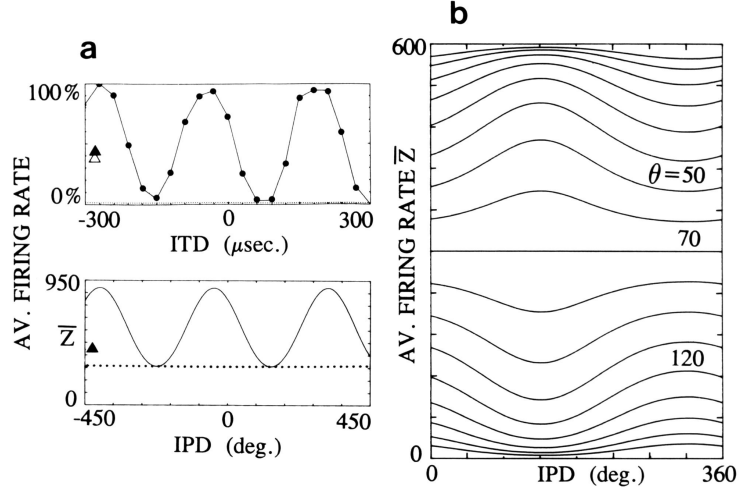


**Figure 4:** (a) Sensitivity to interaural time/phase difference. Upper curve: Experimental ITD-curve of an NL neuron (from 8). Monaural and binaural period histograms of this neuron were shown in Fig. 2 (right). The ITD-curve, which is normalized to the maximum response, was measured at a frequency of 4409 Hz, close to the neuron's best frequency. Lower curve: Model calculation of the IPD-curve (for any given frequency  $f$ , the IPD can be translated into ITD by the simple equation  $IPD = ITD \cdot f \cdot 360^\circ$ ). The dotted lines denote the level of spontaneous activity. The mean values of the experimental ipsi- and contralateral monaural responses are indicated by the solid and open triangles in the upper curve; for the model neuron, both monaural responses are, of course, equal, and are indicated by the single, solid triangle in the lower curve. Observe that in both diagrams the monaural response is about 45% of the response at preferred ITD/IPD, and that the shape of the tuning curves, the preferred phase, the monaural responses, and the relation between spontaneous activity and minimum of the tuning curve are virtually identical in experiment and theory. (b) Model prediction: effects of change in inhibition. With decreasing inhibition, the mean firing rate and, hence, the base level of the IPD-tuning curve increases steadily. Starting at the extreme left of the sigmoid curve, the operating point gradually moves up the expansive region until it crosses the point of inflexion (Fig. 3). The lower set of IPD-curves illustrates how the IPD-sensitivity correspondingly increases from zero until it reaches a maximum, after which it decreases again to vanish completely. If the inhibition decreases even further, the operating point continues into the compressive regime, resulting in a mirror-symmetric set of IPD-curves, however, at progressively higher base level (resulting in generally lower IPD-sensitivity, but also with a non-monotonic behavior) and with a preferred phase difference that has jumped by  $180^\circ$ .

point on the nonlinearity (Equ. 3) and, hence, a change in the degree of asymmetric distortion of the output PH (Fig. 3). Thus, we predict that a decrease in inhibition leads to an increase in the overall firing rate, and, presuming that NL neurons normally operate in the expansive regime, to a (possibly) non-monotonic change in sensitivity to IPD (Fig. 4b). We note in passing that a corresponding shift in the mean firing rate of the NM neurons would have the opposite effect (Equ. 3).

## 5 Discussion

The proposed model explains in detail the binaural period histograms and ITD-curves of physiologically recorded NL neurons. It requires a minimum number of parameters, which can be determined directly from the physiological data. Finally, new physiological experiments with quantitative, testable predictions of the outcome of such experiments can be proposed from the model.

An important role in determining the amount of phase-locking and IPD-tuning of the model NL neuron is played by the inhibition. As far as the anatomy and physiology are concerned, however, this is also the least determined parameter in our model. Anatomical studies have demonstrated the existence of GABA-ergic inputs onto the cell bodies of NL neurons, but as yet there is no clue regarding their origin (14). Physiological studies have provided no direct evidence for inhibition in the NL, let alone of possible phase-locking properties (8). In view of this scant experimental evidence, and although we are aware of the existence of models that rely on the presence of phase-locked inhibition (e.g. 18, 19), we made the minimal assumption possible: inhibition without any phase-locking. The excellent agreement between our theoretical results and the experimental findings supports this view of inhibition as a phase-independent control parameter. Obviously, however, the introduction of more elaborate assumptions, such as inhibition with phase-locking, would function equally well, albeit inevitably at the cost of at least one extra parameter.

A number of alternative models for the computation of ITD has been proposed (10, 18-21). Many of these models implement a coincidence detector in the form of a crosscorrelation: inputs from both sides are multiplied. The best evidence for such multiplication comes from electrophysiological studies in the cat (4, 22) and from psychoacoustics (20). The model proposed here combines the usage of a more biologically oriented, 'soft' threshold with saturation, with a formal representation that includes the crosscorrelation-type models as a special case. Depending on the location of the operating point, the sigmoid nonlinearity has rather different properties (Fig. 3). Thus, the expansive region, which for various reasons qualifies as the normal functional regime, encompasses the multiplicative operation of the crosscorrelator models in a natural way (compare the Taylor expansion). Changing the operating point, however, would cause the transfer function to become first quasi-linear, and eventually compressive. Consequently, our model predicts that an experimental shift of the operating point will result in a change in ITD-tuning (Fig. 4b).

Recently, Colburn et al. (10) proposed a model for the generation of PHs and ITD-curves of MSO neurons, which uses summation of two excitatory inputs, followed by a threshold event generator. Their model, following (23), differs from the present one in several respects. First, it consists of a sequence of two nonlinearities, rather than one: an exponential event generator for each of the two input channels (representing firing of the auditory nerve fibers), followed by a coincidence detector, describing binaural interaction in the MSO neuron. The first nonlinearity, in fact, corresponds to a possible extension of our current model, in which an additional sigmoid nonlinearity is incorporated at the input level to account for 'clipping' in PHs of barn owl NM neurons with best frequencies below 3000 Hz (6, 16, 17). Secondly, the authors point out that their model works without inhibition. However, although inhibition is indeed not incorporated in the second nonlinearity, it is, in fact, present in much the same way as in our model (albeit not explicitly), namely in the setting of the operating point on the input nonlinearities. In this respect, our model is more flexible (and presumably closer to biology), with inhibition at the level of the NL neuron (or, equivalently, in the MSO) allowing for direct manipulation of the binaural interaction process itself, rather than of its inputs. Finally, and most importantly, the Colburn model, in contrast to our system-oriented, probabilistic approach, presents a mechanism-oriented description, based on the interactions

of individual EPSPs at the level of the cell membrane.

The next logical next step in our approach would be to model the underlying biophysical mechanisms, with special emphasis on the constraints imposed by the time constants at various levels. In this context the interesting question arises, how our system-oriented approach can be reconciled with a mechanism-oriented approach, such as presented by the Colburn model. It is our conjecture that an answer to this question can be provided by an appropriate formulation of the rules that govern the statistics of the underlying process (compare the relation between macro-level thermodynamics and micro-level statistical physics). Theoretical as well as experimental research into this issue is currently in progress in our laboratory (24, 25). Meanwhile, it remains striking that a simple, general model of the kind we described, without having to invoke any owl-specific components, accounts for the non-trivial response properties of laminaris neurons when presented with the phase-locked inputs of magnocellular neurons.

**Acknowledgements** Partial funding for this research was obtained from the Bundesministerium für Wissenschaft und Technologie (BMFT; AA, SG), the Deutsche Forschungsgemeinschaft (SFB 307; HW), and from an Alfred P. Sloan fellowship (CC). During the actual writing, one of the authors (AA) was on sabbatical leave in the Dept. of Physiology at the Hebrew University, Jerusalem; he wishes to thank Profs. Moshe Abeles and Eilon Vaadia for their generous hospitality and the German-Israeli Foundation for Research and Development (GIF), the Lady Davis Foundation, and the Minerva Foundation for their support.

## References

1. Jeffress, L. A. (1948) *J. Comp. Physiol. Psych.* 41, 35-39.
2. Goldberg, J. M. & Brown, P. B. (1969) *J. Neurophys.* 32, 613-636.
3. Yin, T. C. T. & Chan, J. C. K. (1988) in *Auditory Function. Neurobiological Bases of Hearing*, eds. Edelman G. M., Gall W. E., & Cowan W. M. (Wiley, New York), pp. 385-430.
4. Yin, T. C. T. & Chan, J. C. K. (1990) *J. Neurophys.* 34, 465-488.
5. Young, S. R. & E. W. Rubel (1986) *J. Comp. Neurol.* 254, 425-459.
6. Sullivan, W. & Konishi, M. (1986) *Proc. Natl. Acad. Sci. USA* 83, 8400-8404.
7. Carr, C. E. & Konishi, M. (1988) *Proc. Natl. Acad. Sci. USA* 85, 8311-8315.
8. Carr, C. E. & Konishi, M. (1990) *J. Neurosci.* 10, 3227-3246.
9. Licklider, J. & Webster, J.C. (1950) *J. Acoust. Soc. Am.* 22, 191-195.
10. Colburn, H. S., Han, Y. & Culotta, C. P. (1990) *Hearing Res.* 49, 335-346.
11. Colburn, H. S. & Durlach, N. I. (1978) in *Handbook of Perception*, eds. Carterette, E. C. & Friedman, M. P. (Academic Press, New York), Vol. 4, pp. 467-518.
12. Little, W. A. (1974) *Math. Biosci.* 19, 101-120.
13. Johannesma, P. I. M. & Van den Boogaard, H. F. P., (1985) *Acta Appl. Math.* 4, 201-224.
14. Carr, C. E., Fujita, I. & Konishi, M. (1989) *J. Comp. Neurol.* 286, 190-207.
15. Takahashi, T. & Konishi, M. (1986) *J. Neurosci.* 6, 3413 - 3422.
16. Grün, S. (1991) MSc. Thesis, University Tübingen (FRG).

17. Aertsen et al., in preparation.
18. Itoh, K. (1984) *Trans. IECE Japan* 67E, 12-18.
19. Lindemann, R. P. (1986) *J. Acoust. Soc. Am.* 80, 1608-1622.
20. Blauert, J. (1983) *Spatial Hearing* (MIT Press, Cambridge).
21. Melssen, W. J., Epping, J. M. & van Stokkum, I. H. M. (1990) *Hearing Res.* 47, 235-256.
22. Yin, T. C. T., Chan, J. C. K. & Carney, L. H. (1987) *J. Neurophysiol.* 58, 562-583.
23. Srinivasan, M. V. & Bernard, G. D. (1976) *Biol. Cybern.* 21, 227-236.
24. Rotter, S. & Aertsen, A. (1991) in *Synapse - Transmission - Modulation*, eds. Elsner, N. & Plenzlin, H. (Thieme, Stuttgart, New York), p. 302.
25. Heck et al., in preparation.